数理解析研究所講究録 第2109巻 2019年 61-69

A Numerical Calculation for Internal Waves over a Slope or a Mound

Taro KAKINUMA

Graduate School of Science and Engineering, Kagoshima University
1-21-40 Korimoto, Kagoshima, Kagoshima 890-0065, JAPAN
taro@oce.kagoshima-u.ac.jp

1. Introduction

Internal waves show interface deformation when they reach a continental shelf after travelling in the deep ocean, as studied by e.g. Ostrovsky & Stepanyants (1989). Grimshaw et al. (2004) numerically simulated the transformation of internal solitary waves using the EKdV eq., obtained by Lee & Beardsley (1974) by extending the KdV eq. However, the applicability of the nonlinear wave equations, derived using perturbation methods for two-layer systems, is restricted owing to the perturbation assumptions, such that, for example, the Benjamin-Ono (BO) equation (Benjamin, 1967; Ono, 1975), as well as the deeper version derived by Choi & Camassa (1999), can be adopted for internal waves in offshore deep regions, while the KdV equation, and the shallower version by Choi & Camassa (1999), for those in shallower water over a continental shelf. In the derivation process for the deeper version by Choi & Camassa (1999), $O(h_1) << O(h_2)$ is assumed, where h_1 and h_2 are the thickness of the upper and lower layers in still water, respectively, while for the shallower version by Choi & Camassa (1999), $O(a/h) = 1$, $O(h_1/l) << 1$, and $O(h_2/l) << 1$ are assumed, where a/h, and l, are the representative values for the ratio between wave height and layer thickness, and wavelength, respectively. Conversely, the set of equations based on a variational principle (Kakinuma, 2001), without any assumption concerning wave nonlinearity or dispersion, is expected to be applicable to nonlinear waves propagating from deep to shallow water, if the vertical distribution of velocity potential is described appropriately.

In the present study, the set of nonlinear equations based on the variational principle, is solved numerically using the implicit scheme developed by Nakayama & Kakinuma (2010), to simulate internal waves in two-layer systems over topography, in consideration of both the strong nonlinearity, and the strong dispersion, of internal waves.

2. Nonlinear equations for surface/internal waves and numerical method

The illustration in Fig. 1 is our schematic for the multi-layer system of fluids, represented as i ($i = 1, 2, \cdots, I$) from top to bottom, respectively, showing only inviscid and incompressible motion. The thickness of the i-layer in still water is denoted by $h_i(\boldsymbol{x})$. None of the fluids mix even in motion, and the density in the i-layer, ρ_i, is spatially uniform and temporally constant in each layer.

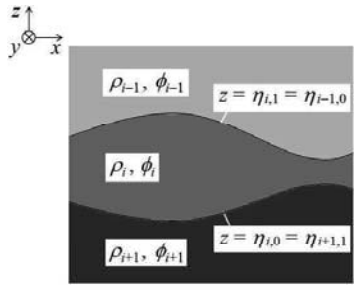

Fig. 1. A schematic for a multi-layer fluid system.

In the *i*-layer, if both the displacement of one interface, $z = \eta_{i,1-j}(\boldsymbol{x},t)$ (j = 0 or 1), and the pressure on the other interface, $p_{i-j}(\boldsymbol{x},t)$, are known, then the unknown variables are the velocity potential $\phi_i(\boldsymbol{x},z,t)$ and the interface displacement $\eta_{i,j}(\boldsymbol{x},t)$, such that the definition of the functional for the variational problem in the *i*-layer, F_i, is as follows (Kakinuma, 2001), by adjusting the functional introduced by Luke (1965):

$$F_i[\phi_i,\eta_{i,j}] = \int_{t_0}^{t_1}\iint_A L_i[\phi_i,\eta_{i,j}]\,dA\,dt, \tag{1}$$

$$L_i[\phi_i,\eta_{i,j}] = \int_{\eta_{i,0}}^{\eta_{i,1}}\left[\frac{\partial\phi_i}{\partial t}+\frac{1}{2}(\nabla\phi_i)^2+\frac{1}{2}\left(\frac{\partial\phi_i}{\partial z}\right)^2+gz+\frac{p_{i-j}+P_i}{\rho_i}\right]dz, \tag{2}$$

where $\eta_{i,0}(\boldsymbol{x},t)$ and $\eta_{i,1}(\boldsymbol{x},t)$ are the displacements of the lower and upper interfaces of the *i*-layer, respectively; $p_{i,0}(\boldsymbol{x},t)$ and $p_{i,1}(\boldsymbol{x},t)$ are the pressures at the lower and upper interfaces of the *i*-layer, respectively; $P_i = \sum_{k=1}^{i-1}(\rho_i-\rho_k)gh_k$; ∇ is a partial differential operator in the horizontal plane, i.e., $\nabla = (\partial/\partial x, \partial/\partial y)$; $(\nabla\phi_i)^2 \equiv |\nabla\phi_i|^2$. The gravitational acceleration g is 9.8 m/s^2. The plane A, which is the orthogonal projection of the object domain on to the *x*-*y* plane, is assumed to be independent of time.

Fluid motion is assumed to be irrotational, resulting in the existence of velocity potential ϕ_i, which is expanded into a power series of vertical position z with weightings f_{i,α_i}, in a manner similar to that for the derivation of surface wave equations by Isobe (1995), as

$$\phi_i(\boldsymbol{x},z,t) = \sum_{\alpha_i=0}^{N_i-1}[f_{i,\alpha_i}(\boldsymbol{x},t)\cdot z^{\alpha_i}] \equiv f_{i,\alpha_i}\cdot z^{\alpha_i}, \tag{3}$$

where N_i is the number of terms for an expanded velocity potential in the *i*-layer.

If we consider a two-layer fluid system, over a seabed of a fixed profile, i.e., $z = \eta_{2,0} = b(\boldsymbol{x})$, then the Euler-Lagrange equations for the variational problem are reduced to the nonlinear surface/internal wave equations for two-layer fluid motion as

[Upper layer]

$$\zeta^{\alpha_1}\frac{\partial\zeta}{\partial t}-\eta^{\alpha_1}\frac{\partial\eta}{\partial t}+\frac{1}{\alpha_1+\beta_1+1}\nabla\left[\left(\zeta^{\alpha_1+\beta_1+1}-\eta^{\alpha_1+\beta_1+1}\right)\nabla f_{1,\beta_1}\right]-\frac{\alpha_1\beta_1}{\alpha_1+\beta_1-1}\left(\zeta^{\alpha_1+\beta_1-1}-\eta^{\alpha_1+\beta_1-1}\right)f_{1,\beta_1}=0, \tag{4}$$

$$\zeta^{\beta_1}\frac{\partial f_{1,\beta_1}}{\partial t}+\frac{1}{2}\zeta^{\beta_1+\gamma_1}\nabla f_{1,\beta_1}\nabla f_{1,\gamma_1}+\frac{1}{2}\beta_1\gamma_1\zeta^{\beta_1+\gamma_1-2}f_{1,\beta_1}f_{1,\gamma_1}+g\zeta=0, \tag{5}$$

$$\eta^{\beta_1}\frac{\partial f_{1,\beta_1}}{\partial t}+\frac{1}{2}\eta^{\beta_1+\gamma_1}\nabla f_{1,\beta_1}\nabla f_{1,\gamma_1}+\frac{1}{2}\beta_1\gamma_1\eta^{\beta_1+\gamma_1-2}f_{1,\beta_1}f_{1,\gamma_1}+g\eta+\frac{p}{\rho_1}=0, \tag{6}$$

[Lower layer]

$$\eta^{\alpha_2}\frac{\partial\eta}{\partial t}+\frac{1}{\alpha_2+\beta_2+1}\nabla\left[\left(\eta^{\alpha_2+\beta_2+1}-b^{\alpha_2+\beta_2+1}\right)\nabla f_{2,\beta_2}\right]-\frac{\alpha_2\beta_2}{\alpha_2+\beta_2-1}\left(\eta^{\alpha_2+\beta_2-1}-b^{\alpha_2+\beta_2-1}\right)f_{2,\beta_2}=0, \tag{7}$$

$$\eta^{\beta_2}\frac{\partial f_{2,\beta_2}}{\partial t}+\frac{1}{2}\eta^{\beta_2+\gamma_2}\nabla f_{2,\beta_2}\nabla f_{2,\gamma_2}+\frac{1}{2}\beta_2\gamma_2\eta^{\beta_2+\gamma_2-2}f_{2,\beta_2}f_{2,\gamma_2}+g\eta+\frac{1}{\rho_2}\left[p+\left(\rho_2-\rho_1\right)gh_1\right]=0, \tag{8}$$

where the surface, and the interface, profiles are described by $z=\eta_{1,1}=\zeta(\boldsymbol{x},t)$, and $z=\eta_{1,0}=\eta_{2,1}=\eta(\boldsymbol{x},t)$, respectively; the pressure at the interface is denoted by $p=p_{1,0}=p_{2,1}$. The sum rule of product is adopted for subscripts α_i, β_i, and γ_i, such that, for example, α_1 in the first term on the left-hand side of Eq. (4) denotes the power of ζ.

After eliminating p from Eqs. (6) and (8), we obtain

$$\begin{aligned}\eta^{\beta_2}\frac{\partial f_{2,\beta_2}}{\partial t}+\frac{1}{2}\eta^{\beta_2+\gamma_2}\nabla f_{2,\beta_2}\nabla f_{2,\gamma_2}+\frac{1}{2}\beta_2\gamma_2\eta^{\beta_2+\gamma_2-2}f_{2,\beta_2}f_{2,\gamma_2}+\left(1-\frac{\rho_1}{\rho_2}\right)g\left(\eta+h_1\right)\\-\frac{\rho_1}{\rho_2}\left(\eta^{\beta_1}\frac{\partial f_{1,\beta_1}}{\partial t}+\frac{1}{2}\eta^{\beta_1+\gamma_1}\nabla f_{1,\beta_1}\nabla f_{1,\gamma_1}+\frac{1}{2}\beta_1\gamma_1\eta^{\beta_1+\gamma_1-2}f_{1,\beta_1}f_{1,\gamma_1}\right)=0.\end{aligned} \tag{9}$$

In this paper, the top face of the upper layer is assumed to touch a fixed horizontal plate at $z=0$, such that $\zeta=0$ without any surface wave. In order to represent both the nonlinearity and dispersion of internal waves propagating from deep to shallow, or shallow to deep, regions, the numbers of terms for the expanded velocity potentials introduce in Eq. (3), are $N_1=3$ and $N_2=5$ for the upper and lower layers, respectively, referring to the accuracy of the numerical results obtained by Yamashita & Kakinuma (2015), using the same equations for the internal solitary waves.

The fundamental equations mentioned above, are solved using the finite-difference implicit scheme developed by Nakayama & Kakinuma (2010). The incident wave is a solitary-wave solution, obtained for the same equations, using the numerical method presented by Yamashita and Kakinuma (2015). In the following discussion, the fluid density ratio ρ_1/ρ_2 is 0.98; in the offshore deep region, the thickness of the upper and lower layers in still water, is $h_1=0.01h$ and $h_2=0.99h$, respectively, where h is the total water depth.

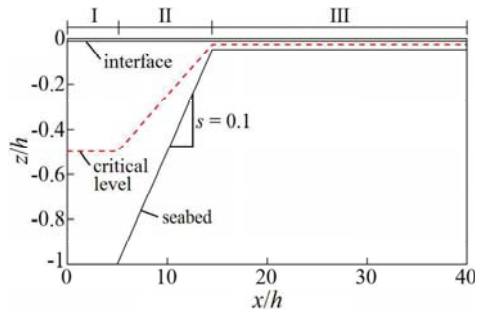

Fig. 2. The target domain with a slope in Case 1-A, where h_2/h_1= 99.0 in the deep area I, while h_2/h_1 = 4.0 in the shallow area III. The broken line shows the critical level z_c, defined by Eq. (10).

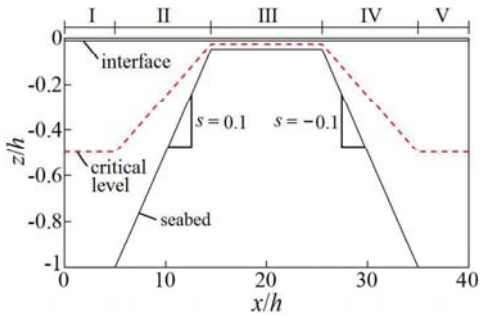

Fig. 3. The target domain with a mound in Case 2-A, where h_2/h_1= 99.0 in the deep area I, while h_2/h_1 = 4.0 in the shallow area III. The broken line shows the critical level z_c, defined by Eq. (10).

Tab.1. The still-water thickness ratios between the lower and upper layers, h_2/h_1, in the shallow area III.

Case	h_2/h_1 in the shallow area III
1-O, 2-O	8.0
1-A, 2-A	4.0
1-B, 2-B	1.0
1-C, 2-C	0.5
1-D, 2-D	0.4

3. Conditions for numerical computation

Figures 2 and 3 show the target domains for computation, where the total water depth is uniform in the areas I, III, and V, while the slope gradient is 0.1 and –0.1 in the areas II and IV, respectively. The still-water thickness ratios between the lower and upper layers, h_2/h_1, in the shallow area III, are shown in Tab. 1. The broken lines in the figures show the elevation of critical level z_c, defined by Funakoshi & Oikawa (1986) as

$$z_c = b\Big/\left(1+\sqrt{\rho_2/\rho_1}\right). \tag{10}$$

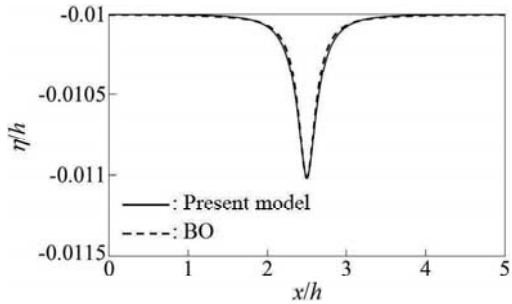

Fig. 4. The interface profile of the incident internal solitary wave, given in the deep area I, in comparison with the corresponding BO solution.

In the deep area I, the interface exists above the critical level, such that downward convex internal waves are stable, while in the shallow area III for Cases 1-C and 1-D, as well as Cases 2-C and 2-D, the interface exists below the critical level, therefore upward convex internal waves are stable.

The grid width, and time step, for computation are $\Delta x = 0.01h$, and $\Delta t = 0.01\Delta x/C_{i,0,I}$, respectively, where $C_{i,0,I}$ is the phase velocity of linear internal waves in the area I, on the assumption that the internal waves propagate in shallow water. The phase velocity of linear internal waves in shallow water, $C_{i,0}$, is evaluated by

$$C_{i,0} = \sqrt{(\rho_2 - \rho_1)gh_1h_2/(\rho_2 h_1 + \rho_1 h_2)}\,. \tag{11}$$

Shown in Fig. 4 is the interface profile of the incident internal solitary wave, given in the deep area I for all the present cases, in comparison with the corresponding BO solution, where the ratio between wave height and upper layer thickness in still water, a/h_1, is 0.1.

4. Internal waves propagating from deep to shallow regions

Figure 5 shows the interface profile at each time in Case 1-O, where $h_2/h_1 = 8.0$ in the shallow area III. The internal wave shows disintegration over the continental shelf in the area III after passing the slope, resulting in two downward convex internal waves.

In Fig. 6, the interface profile at $tC_{i,0,I}/h = 34.9$ in Case 1-A, where $h_2/h_1 = 4.0$ in the shallow area III, is compared with the theoretical solutions for the corresponding internal solitary wave. According to the figure for Case 1-A, although the BO-type downward convex internal wave is stable in the deep area I, the KdV-type downward convex wave appears in the shallow area III.

Figure 7 shows the interface profile at $tC_{i,0,I}/h = 30.5$ in Case 1-B, where $h_1 = h_2$ in the shallow area III. In this case, the internal wave shows instability, leading to a long wave train.

Shown in Fig. 8 is the time variation of the interface profile in Case 1-D, where $h_2/h_1 = 0.4$ in the shallow area III. Partial reflection of the internal wave occurs at the boundary between the areas II and III,

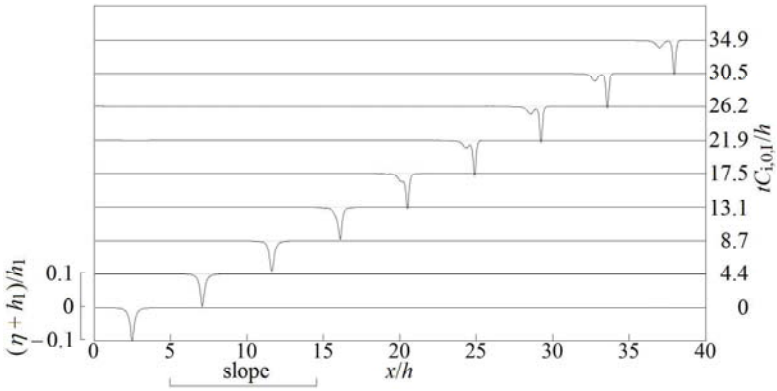

Fig. 5. The time variation of the interface profile in Case 1-O, where $h_2/h_1 = 8.0$ in the shallow area III.

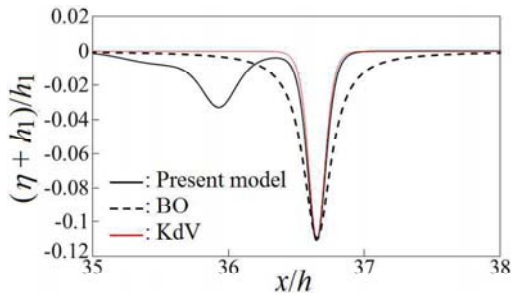

Fig. 6. The interface profile at $tC_{i,0,1}/h = 34.9$ in Case 1-A, where $h_2/h_1 = 4.0$ in the shallow area III, in comparison with the BO and KdV solutions for the corresponding internal solitary wave.

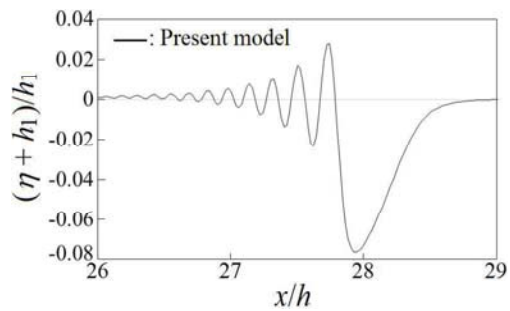

Fig. 7. The interface profile at $tC_{i,0,1}/h = 30.5$ in Case 1-B, where $h_1 = h_2$ in the shallow area III.

owing to the change in slope gradient. The total length of the internal wave train increases as the waves propagate.

Depicted in Fig. 9 is the interface profile at $tC_{i,0,1}/h = 34.9$ in Case 1-C, where $h_2/h_1 = 0.5$ in the shallow area III, in comparison with the KdV solution for the corresponding internal solitary wave. According to the

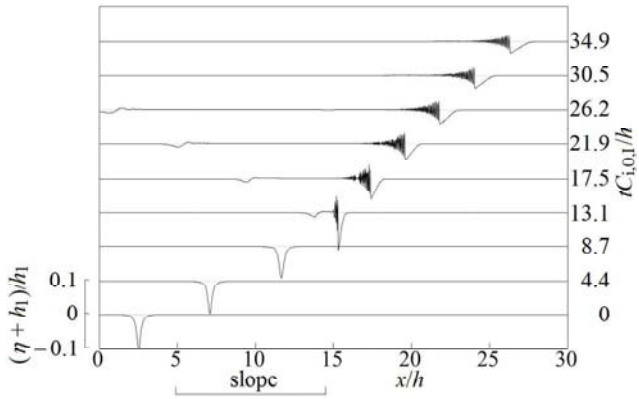

Fig. 8. The time variation of the interface profile in Case 1-D, where $h_2/h_1 = 0.4$ in the shallow area III.

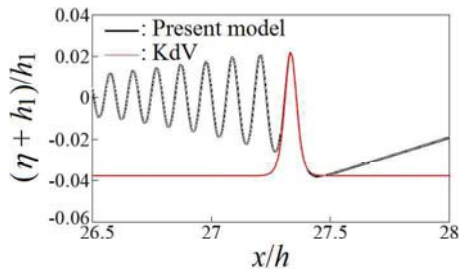

Fig. 9. The interface profile at $tC_{i,0,I}/h = 34.9$ in Case 1-C, where $h_2/h_1 = 0.5$ in the shallow area III, in comparison with the KdV solution for the corresponding internal solitary wave.

figure, the BO-type downward convex internal wave in the deep area has changed to a KdV-type upward convex internal wave in the shallow area, for the interface elevation exceeds the critical level over the slope. The reversal of convex direction, i.e., convex flipping, of internal waves were shown in the numerical results obtained by Helfrich et al. (1984), as well as the field data from the observation by Orr & Mignerey (2003).

Figure 10 shows the relative energy, i.e., the ratios of kinetic and potential energy to the total energy E_i, in Case 1-C, where $h_2/h_1 = 0.5$ in the shallow area III. For instance, $E_{i,K,I+II}$ is the kinetic energy of internal waves in both the deep area I, and the area II with the slope, while $E_{i,P,III}$ is the potential energy of internal waves in the shallow area III. In Case 1-C, the potential energy becomes larger than the kinetic energy for the internal waves in the shallow area III, although the kinetic energy is slightly larger than the potential energy for the incident internal solitary wave in the deep area I.

5. Internal waves propagating over a mound

Internal waves passing through a region over a mound, as shown in Fig. 3, have also been numerically simulated: the lowest elevation of the interfaces at each location is shown in Fig. 11. In Cases 1-A and 2-A,

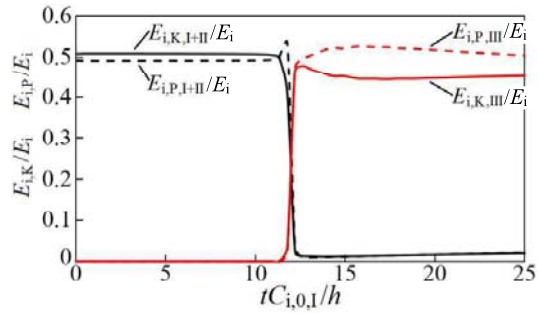

Fig. 10. The relative kinetic and potential energy, i.e., $E_{i,K}/E_i$ and $E_{i,P}/E_i$, respectively, in Case 1-C, where h_2/h_1 = 0.5 in the shallow area III; E_i is the total energy of internal waves. For example, $E_{i,K,I+II}$ denotes the kinetic energy of internal waves in both the areas I and II.

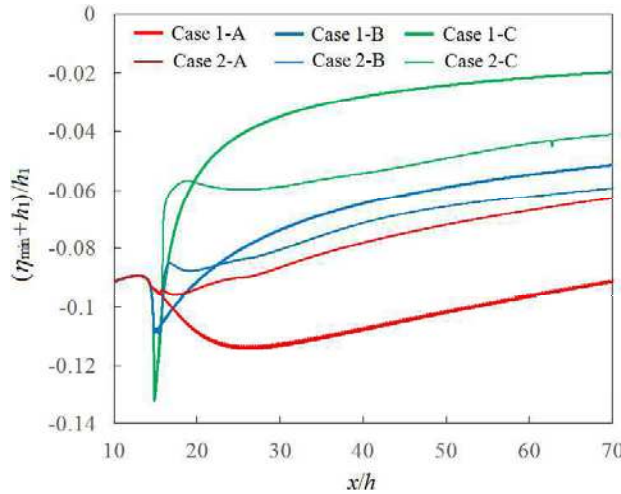

Fig. 11. The distributions of the lowest elevation η_{min} of the interfaces in Cases 1-A, 1-B, and 1-C, where h_2/h_1 = 4.0, 1.0, and 0.5, respectively, in the shallow area III shown in Fig. 1, as well as Cases 2-A, 2-B, and 2-C, where h_2/h_1 = 4.0, 1.0, and 0.5, respectively, in the shallow area III shown in Fig. 2.

where the interface exists above the critical level also in the shallow area III, the lowest elevation of wave-trough interface in Case 2-A is higher than that in Case 1-A at $x/h > 25.0$, which means that the wave height of the first internal wave decreases after its passing the shallow area III. Conversely, the lowest elevation of the interfaces in Cases 2-B and 2-C is lower than that in Cases 1-B and 1-C, respectively, at $x/h > 25.0$.

6. Conclusions

The internal waves propagating from the deep to shallow, or the shallow to deep, areas in the two-layer fluid systems, were numerically simulated by solving the set of nonlinear equations, based on the variational

principle in consideration of both the strong nonlinearity and strong dispersion of internal waves. When the BO-type downward convex internal waves propagated into the shallow areas, the convex direction of interfaces in the shallow areas, depended on the elevational relationship between the interface, and the critical level, in the shallow area. In the cases where the elevation of the still-water interface was below, or equal to, the critical level in the shallow area, the disintegration of internal waves occurred remarkably, leading to a long wave train. When the internal wave travelled in the deeper area after passing the shallow area, the wave height decreased when the interface elevation is higher than the critical level also in the shallow area.

Acknowledgments

This work was supported by both JSPS Grant-in-Aid for Scientific Research (B) Grant Number JP17H02856, and (C) Grant Number JP17K06585.

References

Benjamin, T. B.: Internal waves of permanent form in fluids of great depth, J. Fluid Mech., Vol. 29, pp. 559-592, 1967.

Choi, W. and Camassa, R.: Fully nonlinear internal waves in a two-fluid system, J. Fluid Mech., Vol. 396, pp. 1-36, 1999.

Funakoshi, M. and Oikawa, M.: Long internal waves of large amplitude in a two-layer fluid, J. Phys. Soc. Jpn, vol. 55, pp. 128-144, 1986.

Grimshaw, R., Pelinovsky, E., Talipova, T. and Kurkin, A.: Simulation of the transformation of internal solitary waves on oceanic shelves, J. Phys. Oceanogr., Vol. 34, pp. 2774-2791, 2004.

Helfrich, K. R., Melville, W. K. and Miles, J. W.: On interfacial solitary waves over slowly varying topography, J. Fluid Mech., Vol. 149, pp. 305-317, 1984.

Isobe, M.: Time-dependent mild-slope equations for random waves, In Coastal Eng. 1994, pp. 285-299, 1995.

Kakinuma, T.: A set of fully nonlinear equations for surface and internal gravity waves, Proc. 5th Int. Conf. on Computer Modelling of Seas and Coastal Regions, Wessex Insti. Tech. Press, pp. 225-234, 2001.

Lee, C.-Y. and Beardsley, R. C.: The generation of long nonlinear internal waves in a weakly stratified shear flow, J. Geophys. Res., Vol. 79, No. 3, pp. 453-462, 1974.

Luke, J. C.: A variational principle for a fluid with a free surface, J. Fluid Mech., Vol. 27, pp. 395-397, 1967.

Nakayama, K. and Kakinuma, T.: Internal waves in a two-layer system using fully nonlinear internal-wave equations, Int. J. Numer. Meth. Fluids, Vol. 62, pp. 574-590, 2010.

Ono, H.: Algebraic solitary waves in stratified fluids, J. Phys. Soc. Jpn., Vol. 39, pp. 1082-1091, 1975.

Orr, M. H. and Mignerey, P. C.: Nonlinear internal waves in the South China Sea: Observation of the conversion of depression internal waves to elevation internal waves, J. Geophys. Res., Vol. 108, No. C3, pp. 9-1-9-16, 2003.

Ostrovsky, L. A. and Stepanyants, Yu. A.: Do internal solitons exist in the ocean?, Rev. Geophys, Vol. 27, pp. 293-310, 1989.

Yamashita, K. and Kakinuma, T.: Properties of surface and internal solitary waves, In Coastal Eng. 2014, waves. 45, 15 pages, 2015.